









A dietary polyphenol metabolite alters CA1 excitability *ex vivo* and mildly affects cortico-hippocampal field potential generators in anesthetized animals

Marta Montero-Atalaya ^{1,†}, Sara Expósito ^{2,†}, Ricardo Muñoz-Arnaiz ², Julia Makarova ², Begoña Bartolomé ¹, Eduardo Martín ², María Victoria Moreno-Arribas ¹, Oscar Herreras ^{2,*}

¹Dept Biotecnología y Microbiología de Alimentos, Institute of Food Science Research (CIAL), CSIC-UAM, c/Nicolás Cabrera, 9, 28049 Madrid, Spain,

²Dept Neurociencia Translacional, Cajal Institute, CSIC, Av Doctor Arce 37, 28002 Madrid, Spain

*Corresponding author: Cajal Institute–CSIC, Av. Dr. Arce 37, Madrid 28002, Spain. Email: herreras@cajal.csic.es

†Marta Montero-Atalaya and Sara Expósito contributed similarly.

Dietary polyphenols have beneficial effects in situations of impaired cognition in acute models of neurodegeneration. The possibility that they may have a direct effect on the electrical activity of neuronal populations has not been tested. We explored the electrophysiological action of protocatechuic acid (PCA) on CA1 pyramidal cells *ex vivo* and network activity in anesthetized female rats using pathway-specific field potential (FP) generators obtained from laminar FPs in cortex and hippocampus. Whole-cell recordings from CA1 pyramidal cells revealed increased synaptic potentials, particularly in response to basal dendritic excitation, while the associated evoked firing was significantly reduced. This counterintuitive result was attributed to a marked increase of the rheobase and voltage threshold, indicating a decreased ability to generate spikes in response to depolarizing current. Systemic administration of PCA only slightly altered the ongoing activity of some FP generators, although it produced a striking disengagement of infraslow activities between the cortex and hippocampus on a scale of minutes. To our knowledge, this is the first report showing the direct action of a dietary polyphenol on electrical activity, performing neuromodulatory roles at both the cellular and network levels.

Key words: protocatechuic acid (PCA); hippocampus; evoked potentials; field potential generators; polyphenols.

There is evidence that a polyphenol-rich diet plays an important role in the prevention of neurodegenerative diseases, cardiovascular accidents, and stroke. It also appears to improve the cognitive deficits associated with aging and those related to malnutrition in children (Spencer 2009; Yusufov et al. 2017; McGrattan et al. 2019; Román et al. 2019; Roberts et al. 2020). These phenomena have been at least partially associated with the vascular effects of consumed polyphenols, which include angiogenesis or increased blood flow (Figueira et al. 2017, 2019). In addition, a number of effects on signaling pathways have been reported at the cellular level (Khan et al. 2015; Thakare et al. 2017). However, it is unknown whether such effects are mediated by cellular/metabolic pathways or by altering electrical activity in specific brain structures.

Protocatechuic acid (3,4-dihydroxybenzoic acid; PCA) is one of the main metabolites of complex polyphenolic compounds like anthocyanins and flavan-3-ols, phenols that have been widely studied for their beneficial impact on human health through their anti-inflammatory, antitumoral, immunoregulatory, and neuroprotective effects (Krzysztoforska et al. 2019; Song et al. 2020). Moreover, several studies have demonstrated the ability of some of these metabolites to cross the blood–brain barrier (Zhang et al. 2011), suggesting that they might be responsible for the protective effects (Ho et al. 2013; Shimazu et al. 2021).

There have been few studies into the electrophysiological effects of polyphenols and in general, they have focused on very specific phenomena like long-term potentiation (Hajipour et al. 2016; Kim et al. 2022). Given the slow temporal dynamics of the cognitive and pathological events in which polyphenols have been implicated, in addition to exploring direct electrophysiological effects it would be particularly relevant to explore any sustained and long-term changes to electrical activity. Indeed, such alterations have been shown to play an important role in some neurodegenerative diseases like Parkinson's and Alzheimer's disease (Helmich et al. 2013; Nakazono et al. 2018). Therefore, an additional objective of this study was to explore the effects of PCA on electrophysiological activity in the hippocampus and cortex of anesthetized adult rats. These structures were chosen as they are critically involved in memory processes, and they are also significantly affected by stroke and neurodegenerative diseases in which polyphenols have been shown to have a favorable effect (Carecho et al. 2021; Carregosa et al. 2021).

Combining *ex vivo* and *in vivo* studies let us also consider reported antagonistic effects (oxidant-antioxidant) (Song et al. 2020) that might relate to the route of administration. Thus, we tested PCA by (i) direct delivery using hippocampal slices and (ii) through systemic intraperitoneal delivery enabling this

Received: February 16, 2023. Revised: July 17, 2023. Accepted: July 18, 2023

© The Author(s) 2023. Published by Oxford University Press. All rights reserved. For permissions, please e-mail: journals.permission@oup.com.

This is an Open Access article distributed under the terms of the Creative Commons Attribution Non-Commercial License (<https://creativecommons.org/licenses/by-nc/4.0/>), which permits non-commercial re-use, distribution, and reproduction in any medium, provided the original work is properly cited. For commercial re-use, please contact journals.permissions@oup.com

compound to be transported to and metabolized in the brain. The effects on membrane excitability and synaptic transmission were explored in CA1 pyramidal cells intracellularly recorded in whole-cell mode of patch-clamp technique. On the other hand, since the expected action of exogenous compounds involved in processes taking place over long periods is expected to have a sustained action, we wondered if we could detect subtle and sustained drug-induced changes in the ongoing electrical activity of neural networks. On this purpose we used high density linear arrays to record across the cortex and hippocampus, and we employed a spatial discrimination technique as the independent component analysis (ICA) (Bell and Sejnowski 1995) optimized for intracranial field potential (FP) recordings (Herreras et al. 2015) that separates the component FP generators that mix in raw FPs. The time course of FP generators is no longer distorted by mutual contamination between the coactive sources (Herreras 2016). Hence it enables an accurate quantitative assessment at different time scales, i.e. waves, patterns, and trends (Enriquez-Barreto et al. 2014). Also, they provide information on connectivity, since the FP generators have been formerly characterized in these structures and most are pathway-specific (Korovaichuk et al. 2010; Herreras et al. 2015; Torres et al. 2019).

The results obtained indicate that PCA produces an effective modulation of electrophysiological activity in the brain. We observed a significant reduction in the firing capacity of CA1 neurons in response to synaptic excitation or current pulses when exposed to PCA in slices. Additionally, sustained effects of systemic PCA included the disengagement of cortico-hippocampal FP activities at the minute scale.

Methods

All experiments were performed in accordance with EU (2010/63/UE), Spanish (RD 53/2013), and local (Autonomous Community of Madrid, Order 4/8/1988) regulations regarding the use of laboratory animals, and the experimental protocols were approved by the Research Committee of the Cajal Institute. Four young female (21–24 days old) and 14 adult female Sprague–Dawley rats of between 3 and 4 months were used for *ex vivo* and *in vivo* experiments, respectively. Animals were inbred at the local animal facilities in a 12-h light/dark cycle, stable temperature (20–22°C), and food (Teklad-2018) and water were given *ad libitum*.

We followed the ARRIVE Essential 10 guidelines to report on animal research. The experimental unit is an individual animal. Animals for *in vitro* experiments were from the same litter while those for *in vivo* experiments were selected from different litters and randomly assigned to the different groups ($n=6$ individuals per group). Sample size was determined according to former studies exploring the number of pathway-specific FP generators in the hippocampus (Herreras et al. 2015). The activity within these generators varies over time and cannot be homogenized across animals (Enriquez-Barreto et al. 2014), hence it cannot be used to determine sample size. Electrophysiological data are hosted on the servers of the Cajal Institute, and may be available for research purposes upon request and subjected to the CSIC institutional regulations. Data analysis was blindly performed by researchers other than those who executed procedures.

Ex vivo experiments

Coronal hippocampal slices (350 μM) were prepared from 21–24 days old rats. The animals were decapitated, and their brains were quickly sliced in ice-cold artificial cerebrospinal fluid (ACSF) using a vibratome (Vibratome Series 3000 Plus, St. Louis). Slices containing the hippocampal formation were incubated

for 1 h at room temperature (21–24°C) in ACSF that contained 124 mM NaCl, 2.69 mM KCl, 1.25 mM KH_2PO_4 , 2 mM MgSO_4 , 26 mM NaHCO_3 , 2 mM CaCl_2 , and 10 mM glucose. The ACSF was continuously gassed with 95% O_2 and 5% CO_2 to maintain a pH of 7.3. Subsequently, the slices were transferred to an immersion recording chamber and superfused at a rate of 2 mL/min. All chemicals were purchased from Sigma-Aldrich.

Electrophysiological recordings of CA1 pyramidal neurons were made in whole-cell configuration of patch-clamp technique. Patch electrodes were fabricated from borosilicate glass capillaries with a micropipette puller (Brown-Flaming model P-90, Sutter Instruments, Novato, CA). Pipettes with resistances of 4–10 $\text{M}\Omega$ were filled with an internal solution that contained (in mM): 135 KMeSO_4 , 10 KCl, 10 HEPES, 93.5 NaCl, 5 EGTA, 10 phosphocreatine, 2.5 ATP- Mg^{+2} , and 0.3 GTP- Na^+ , with an equilibrated pH = 7.3–7.4. Electrophysiological recordings were obtained from one neuron per slice and 3–4 slices per rat with controlled temperature (32–36°C) using a Multiclamp 700B amplifier. Data were acquired using a Digidata 1550B and analyzed using a digital system (pClamp version 11.2, Molecular Devices) with a sampling rate of 10 kHz. To assess the intrinsic excitability of CA1 pyramidal neurons, a series of depolarizing currents of 500 ms were injected through the patch electrode in current clamp mode stepping from –15 to 270 pA. Rheobase was measured as the threshold current level required to elicit a spike. The spike threshold was detected as the membrane potential at which first order derivatives (dV/dt) of the spike exceeded 15 mV/ms. Peak amplitude was measured from threshold to the peak of the spike. Spike half-width was calculated as the duration at half amplitude between the baseline and the peak. Phase plots were constructed by plotting the somatic membrane potential versus the time derivative of the somatic membrane potential (dV/dt) of the first spike.

Excitatory postsynaptic potentials (EPSPs) were recorded from CA1 pyramidal neurons after assessing their intrinsic excitability properties. EPSPs were evoked by stimulation of the apical or basal dendritic trees with an extracellular bipolar tungsten electrode placed in the stratum radiatum or the stratum oriens, respectively, via a 2100 isolated pulse stimulator (A-M Systems, Inc., Carlsborg, WA). Monopolar square pulses of 50 μs of duration with increasing intensity were applied until a spike was generated.

In vivo experiments

Experiments were performed in the dorsal hippocampus and the overlying cortex of individual animals anesthetized with urethane (1.5 g/kg, *i.p.*) and fastened to a stereotaxic device, maintaining their body temperature at $37 \pm 0.1^\circ\text{C}$. Surgical and stereotaxic procedures were performed as described previously (Ortuño et al. 2019). Concentric stimulating electrodes (TM33CCNON, WPI) were placed in the CA3b soma layer (in mm from bregma: AP-3.2; LM ± 2.6 ; V-3.3) to activate the Schaffer input to the CA1. Stimuli (0.07–0.1 ms square pulses) were delivered at 0.1 Hz. Recording was made through multisite probes (see below) connected to a headstage. A subcutaneous Ag/AgCl wire under the skin of the neck was used as reference, and the signals were amplified and acquired using a MultiChannel System (Reutlingen, Germany) or Open Ephys hardware and software (20 kHz sampling rate).

At the end of each experiment the animals were perfused through the abdominal aorta with PBS containing heparin (0.1%) followed by paraformaldehyde (4%). Sagittal brain sections (100 μm) were then stained with bis-benzimide and the electrode position was assessed by fluorescence microscopy.

Experiments were designed to explore the effects of systemic administration of PCA (Sigma Aldrich, ref. P-5630, CAS number 99-50-3) (*i.p.*, 150 mg/kg dissolved in NaCl 0.9% with dymethyl

sulfoxide [DMSO] 1%). This concentration was selected based on comparative studies of the effects of PCA on brain induced-damage in rats (doses of 10–50 mg/kg for direct and intraperitoneal administration) (Kale et al. 2021) and existing evidence of brain uptake and plasma levels of phenolic metabolites generated following the ingestion of polyphenol-rich foods (Gasperotti et al. 2015; Cueva et al. 2017; Carecho et al. 2021).

To test the effects of PCA on network activity, spontaneous laminar FPs were recorded through one multisite linear probe (32 sites, 100 μm : from Atlas, Leuven, Belgium, or Neuronexus, Ann Arbor, MI) that spanned the lower layers of the visual cortex (V2), as well as the CA1 and Dentate Gyrus (DG) hippocampal subfields. Orthodromically evoked potentials in the CA1 were also obtained, for which the population spike (PS) and field excitatory postsynaptic potential (fEPSP) were chosen from optimal sites on the array. In the st. pyramidale, the PS was measured from the precedent positive hump to the peak of the negative limb. In the st. radiatum, the fEPSP was measured as the maximum slope in the negative going limb (Herreras 1990).

Wideband FPs (0.1 Hz–5 KHz) were recorded in consecutive 3 min periods and we focused on irregular hippocampal activity, which is the dominant state at the anesthetic dosage used here (Torres et al. 2019). When the animal displayed frequent theta episodes before drug testing, anesthesia was supplemented (a 10–20% increase of the initial dose) and the animal was allowed to stabilize for 10 min. Occasional theta episodes still occurred during testing, and they were considered to assess their potential impact on the statistical properties of the baseline activity in FP generators (see below).

Spatial discrimination of pathway-specific components in FPs

In the brain, spontaneous FPs are driven by multiple co-activating synaptic sources whose potentials spread and mix in the volume, provoking mutual distortion (Herreras 2016). We used the ICA to separate these components (Korovaichuk et al. 2010; Makarova et al. 2010), each of which has a unique spatial profile that enables its identification and anatomical matching (Benito et al. 2014) (see Herreras et al. 2015, for applications and restrictions). In this study we employed the kernel density ICA algorithm (KDICA) (Chen 2006) that is usually implemented in MATLAB. Briefly, the $u_m(t)$ signals recorded are considered as the weighted sum of the activities of N neuronal sources or FP generators:

$$u_m(t) = \sum_{n=1}^N V_{mn} s_n(t), \quad m = 1, 2, \dots, M$$

where (V_{mn}) is the mixing matrix derived from the so-called voltage loadings or spatial weights of N FP generators on M electrodes, and $s_n(t)$ is the time course of the n -th FP generator. Using $u_m(t)$, the ICA finds both (V_{mn}) and $s_n(t)$. Experimentally and through realistic computer models, it has been shown previously that the time course of a FP-generator $s_n(t)$ corresponds to a postsynaptic temporal convolution of spike output in a population afferent to that recorded (Makarova et al. 2011; Fernández-Ruiz et al. 2012). Typically, only 5–6 components (out of 32 possible) reach significant variance. This enables prior dimension reduction through a principal component analysis (PCA). Typically, maintaining the 6–8 main PCA components optimizes ICA performance in recordings that span the dorsal CA1 and the DG (Benito et al. 2016). We routinely discarded noisy components with a total compound variance below 1% (i.e. always keeping 99% of the original FP variance). Although the FP generators repeated in every animal,

the relative variance varied depending on the precise placement of the array. Thus, we used normalized data for each FP generator to evaluate drug effects.

Once extracted, each FP generator can be analyzed independently in the time or frequency domains. The power of the FP components was estimated at the site where each showed maximal amplitude. The time evolution of the power of an FP generator (in mV^2) was calculated by:

$$P(t) = \int H(t - \tau) v^2(\tau) d\tau, \quad H(x) = \begin{cases} 1/\Delta & \text{if } x \in [-\Delta/2, \Delta/2] \\ 0, & \text{otherwise} \end{cases}$$

where $v(t)$ is the virtual FP at the electrode with maximal power and Δ is the length of averaging. The overall mean power is then defined by setting Δ equal to the complete time interval.

We estimated the periodogram power spectral density (PSD) of the temporal activation of FP generators (power spectra) and then computed the signal power in different frequency bands: delta (δ), <3 Hz; theta (θ), 3–8 Hz; alpha (α), 8–16 Hz; beta (β), 16–25 Hz; gamma (γ), 30–80 Hz. Also, we estimated the number of waves per unit time for each treatment and FP generator. Four classes of amplitude were enabled by setting voltage thresholds at different levels in both positive and negative values (in times the standard deviation: 0.5σ , σ , 2σ , 3σ).

The running power of theta was assessed to account for any potential bias in the effects of PCA on various electrophysiological parameters. Theta power was measured within the FP generator peaking at the st. lacunosum-moleculare (L-M), known to be responsible for this activity (as shown below). This approach prevented the inclusion of theta energy contributed by isolated theta-duration waves from remote sites through volume conduction. To estimate the running power of theta, a 3–5 Hz selected band in the wavelet spectra for this specific generator was utilized, avoiding capturing energy in other frequency bands present in the generator. The entire epoch was divided into fifty consecutive segments, and the mean power was calculated for each segment (resulting in 12–13 consecutive windows per treatment).

Since both native FPs and FP generators are mesoscopic signals, estimating power in frequency bands may not have a direct physiological translation, as it relies on the rate and grouping of microscopic elementary currents (Herreras 2016; Herreras et al. 2022). Therefore, to overcome this limitation, we adopted an additional approach by analyzing the statistical distribution of voltage values in the generator's time course through histograms of the amplitude distribution. Different parameters were estimated using built in functions in MATLAB, as the mean, standard deviation, kurtosis, and skewness. These parameters may detect changes that do not strictly pertain to the mesoscopic level or the frequency domain.

To minimize bias stemming from possible changes in the electrographic state during the sequence of treatments, which could potentially confound the effects of PCA, we constructed a unified population distribution of time values for each generator. This unified distribution contained equivalent time points after each injection, including ACSF, DMSO, PCA, and a recovery period (Post). To achieve this, we normalized the mean and standard deviation of the data from each animal and generator and pooled them together. Subsequently, we assessed the Pearson correlation between each distribution parameter and the power of theta for each generator, considering the presence of theta as a proxy for an electrographic change of state. Next, we compared the values of distribution parameters obtained for each generator after the

vehicle injection to those observed after the PCA injection, allowing us to analyze the specific effects of PCA on each generator relative to the control condition.

Statistical analysis

Statistical analyses were performed using GraphPad Prism version 7.00 for Windows (La Jolla, California, USA). Data are expressed as mean \pm standard error of the mean (s.e.m.). The normality of the data was assessed using the Shapiro–Wilk test and the homogeneity of variances was checked with the Levene test. For *ex vivo* results we used Student's *t*-tests and one or two-way ANOVA, and were followed by post-hoc comparisons with Bonferroni or Tukey as deemed appropriate. The experiments involving *i.p.* injections had three levels of qualitative variables (CTRL, DMSO, and PCA) and hence, multiple-way ANOVA or Kruskal Wallis test were performed, followed by the Bonferroni's post-hoc test. *P*-value and test employed are reported in the figure legends. Statistical differences were established with $P < 0.05$ (*), $P < 0.01$ (**), and $P < 0.001$ (***)

The ICA is a higher order statistic and the number of FP generators returned may vary from one sample to another depending on the animal's processing demands. We rejected all components that contributed $< 1\%$ of the total variance (Makarova et al. 2011). The mean power of the component or their frequency content was compared for each of the treatments (Control 3 min, DMSO 30 min, PCA 40 min) and among individuals ($n = 6$ animals). The same statistical tests were used as indicated above.

Results

PCA increases synaptic responses *ex vivo* more in basal than apical dendrites

We analyzed the evoked activity of individual CA1 pyramidal neurons recorded in whole-cell mode (Fernández et al. 2010). We investigated the effects before and after adding PCA at a concentration of $10 \mu\text{M}$ to the bath, along with DMSO at $10 \mu\text{M}$. At this concentration, DMSO alone had no evident effect. All analyzed cells exhibited a stable resting membrane potential, with the mean value being $V_m = -61.5 \pm 0.48 \text{ mV}$ ($n = 15$). Synaptic responses were measured at the cell soma upon activation of either the apical dendrites through the Schaffer collateral/commissural input in the st. radiatum or basal dendrites by afferents in the st. oriens (Fig. 1A). Supra-threshold EPSPs evoked a single action potential (AP). Upon the addition of PCA, there was a noticeable enlargement of the synaptic potential upon activation of the apical afferents. However, the peak amplitude was only minimally affected (Fig. 1B). Therefore, we evaluated the EPSP area and EPSP half-width (Fig. 1C), both of which exhibited a significant increase during PCA across the range of stimuli. The effect of PCA was even more pronounced in the basal dendrites, where the EPSP amplitude grew to nearly double its size before PCA (Fig. 1D and E). Importantly, the enlargement of the EPSP occurred with little or no change in the rising phase, indicating that the effect may be primarily on the EPSP repolarization during its course toward the soma rather than at the synaptic loci (see insets in Fig. 1B and D).

PCA strongly reduces evoked cell firing by a change of rheobase

Despite the notable increase and enlargement of the evoked EPSPs, cell firing was significantly reduced during PCA, regardless of apical or basal excitation (as shown in the histograms in Fig. 1B and D, respectively). For instance, the firing probability for the strongest intensity decreased from $57.1\% \pm 10.8$ to $13.3\% \pm 2$

after apical activation and from $33\% \pm 6.7$ to $13\% \pm 2.6$ after basal activation (mean \pm s.e.m.).

To further explore the contrasting behavior of synaptic and spike-evoked responses, we examined the intrinsic excitability by injecting depolarizing current pulses in current clamp mode. The spike firing frequency (Fig. 2A) was measured by counting spikes during the 500 ms depolarizing pulse (six pulses were averaged for each cell and condition). Notably, we observed a drastic reduction in cell firing during PCA perfusion compared to the control condition (Fig. 2A; $P < 0.001$; two-way ANOVA, $F(1, 280) = 632.1$). Additionally, three out of fifteen neurons failed to fire upon the largest current injection. Furthermore, both the rheobase (current threshold) and the voltage threshold (Fig. 2B) required to elicit a spike exhibited significantly higher values during PCA. The rheobase increased from $89 \pm 8.6 \text{ pA}$ in the control condition to $143 \pm 17.9 \text{ pA}$ during PCA (see statistics in the figure). Similarly, the voltage threshold increased from $-45 \pm 0.6 \text{ mV}$ in control to $-39 \pm 1.2 \text{ mV}$ during PCA.

Parameters such as spike half-width and peak amplitude were also evaluated (Fig. 2C), but no significant differences were observed between conditions. Additionally, we examined the rising slope of the spike, which is primarily shaped by Na^+ currents in the soma and axon hillock. During PCA, most cells (9 out of 13) exhibited a consistent reduction in the rising slope, two cells showed an increase, and two others remained unchanged (Fig. 2D, left). Due to the individual data dispersion, the population statistics did not reach significance ($P = 0.33$, paired *t*-test).

To gain further insights, we normalized the time course by the amplitude of the first spike across all cells and calculated the average phase plot under control and PCA conditions (Fig. 2D, right). The voltage threshold was evident by a right-ward shift of the departing point (indicated by the dashed oval), while a subnormal course of the initial phase during PCA suggested a considerable reduction in the rising slope (indicated by the downward arrows). The slope reduced from $262.9 \pm 18.9 \text{ V/ms}$ in control to $236.1 \pm 18.8 \text{ V/ms}$ during PCA.

Overall, these findings point to a multifaceted effect of PCA on intrinsic properties and cell domains, highlighting the complex impact of PCA on CA1 pyramidal neurons.

Systemic delivery of PCA enhances Schaffer-CA1 excitatory transmission

We also explored whether systemic delivery of PCA had any effect on electrophysiological parameters in the hippocampus of anesthetized animals, assessing the Schaffer-CA1 evoked potentials (Fig. 3A). We chose an intensity that elicited an o-PS about one third of the maximum, which allowed amplitude changes in any direction to be detected, although it also yielded significant spontaneous fluctuations, including those related to the occurrence of theta epochs (Fig. 3B). All the responses were averaged over 1-min periods ($n = 6$). After a 3 min control recording, DMSO (1%) was injected (*i.p.*) and 30 min later, a single dose of PCA (150 mg/kg *i.p.*) was delivered. While DMSO produced no significant effect on the fEPSP or the o-PS, PCA increased both potentials (expressed as the % of the control 3 min post injection): fEPSP, 114.6 ± 17.1 after DMSO versus 128 ± 30.2 after PCA ($n = 12$, $P = 0.347$, Mann Whitney); o-PS, 115.4 ± 19.2 after DMSO versus 128.1 ± 31.2 after PCA ($n = 12$, $P = 0.219$; Fig. 1B and C). A mild run-down was associated with this effect that reduced the statistical significance after a few minutes, although the enhancement was evident up to 30 min post injection.

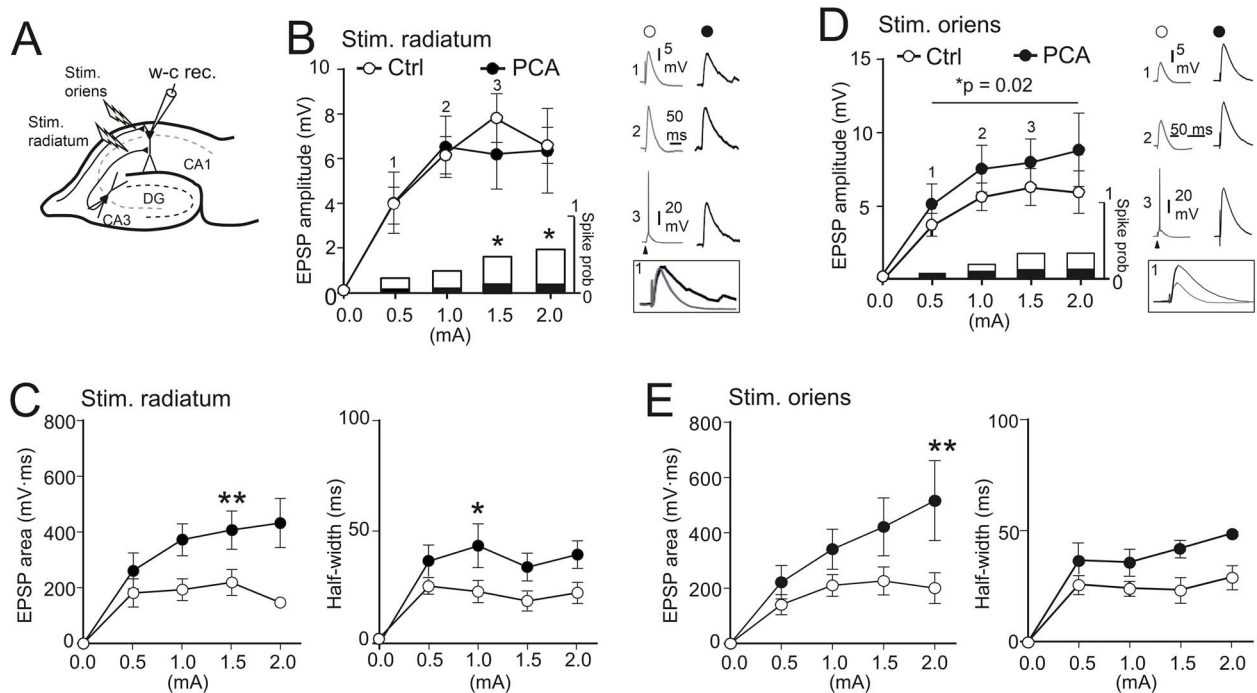


Fig. 1. PCA impairs spike generation despite increased synaptic responses. (A) Scheme of electrode arrangement. Whole-cell patch clamp recordings were made from the soma of CA1 pyramidal neurons ($n = 15$). EPSPs were induced by orthodromic stimulation of apical dendrites through the Schaffer pathway in the st. radiatum (B, C), or the basal dendrites in the st. oriens (D, E). (B) *Left*: PCA $10 \mu\text{M}$ perfusion in the bath decreases the probability of AP initiation (bar histogram) even with no changes in EPSP amplitude (line plots). *Right*: Examples of evoked EPSPs at different intensities, some of them followed by an AP. Arrowhead indicates time of stimulation. (C) Comparisons of the area and half-width of the EPSPs evoked by st. radiatum stimulation between control and PCA conditions. Two-way ANOVA followed by Bonferroni test. (D) *Left*: Same stimulation protocol as in (B) but using a stimulation electrode placed in the st. oriens. Again, bath perfusion of PCA prevents the generation of spikes [two-way ANOVA, $F(8, 8) = 1,797$; post-hoc comparison with Bonferroni test] despite larger EPSP amplitudes (two-way ANOVA, $F(4, 85) = 14,31$; post-hoc comparison with Bonferroni test). *Right*: Examples of evoked EPSPs at different intensities. The insets in B and D show the superposition of traces in examples labeled 1. (E) Same as in (C) but with st. oriens stimulation.

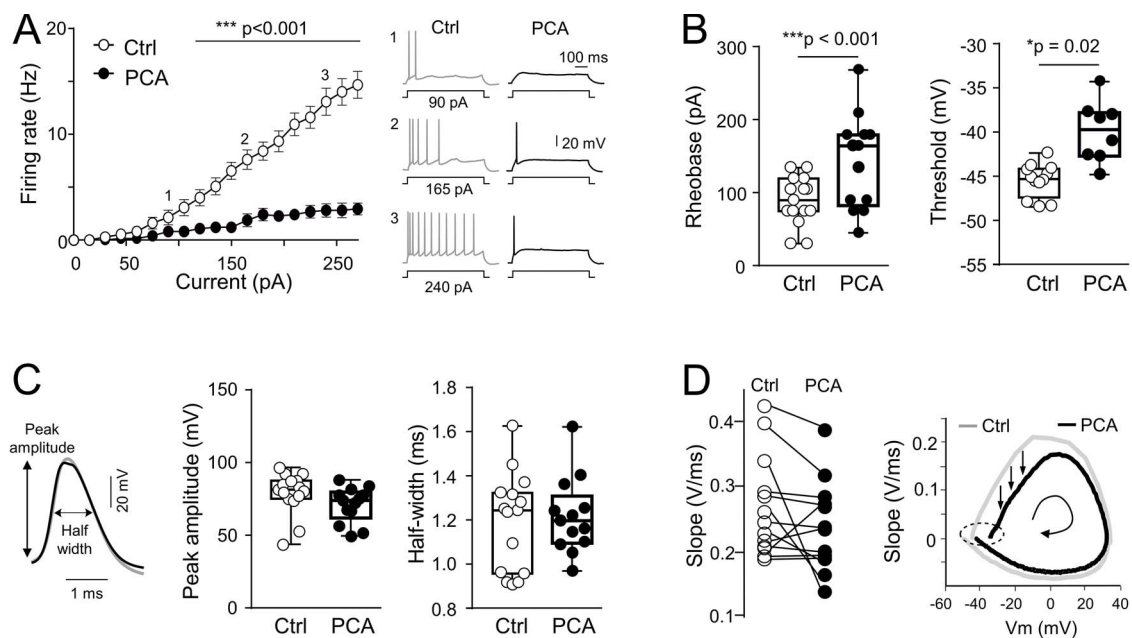


Fig. 2. Hippocampal CA1 neurons exposed to PCA exhibit a decline in intrinsic excitability. (A) Analysis of AP frequency generated by depolarizing pulses (shown from 0 pA to 270 pA, 500 ms) in the absence (ctrl) and presence of PCA $10 \mu\text{M}$ in hippocampal neurons ($n = 15$). Traces of the current-frequency relationship in a representative neuron are shown to the right. (B) AP rheobase and voltage threshold measured from CA1 pyramidal neurons indicates a depolarizing shift after PCA perfusion in the bath. Paired t-tests. (C) Amplitude and half-width of APs elicited by somatic current injections show no difference when applying PCA to the bath. Paired t-tests. (D) *Left*: Most cells showed a reduction of the AP rising slope measured in the first AP appearing upon depolarizing current pulses. *Right*: Phase plot of the normalized first spike averaged across the cell population obtained in control and PCA conditions. Note the positive shift of threshold for APs on application of PCA (dashed oval). An increase of the rising slope also becomes evident (downward arrows). The rounded arrow indicates the time course of the AP.

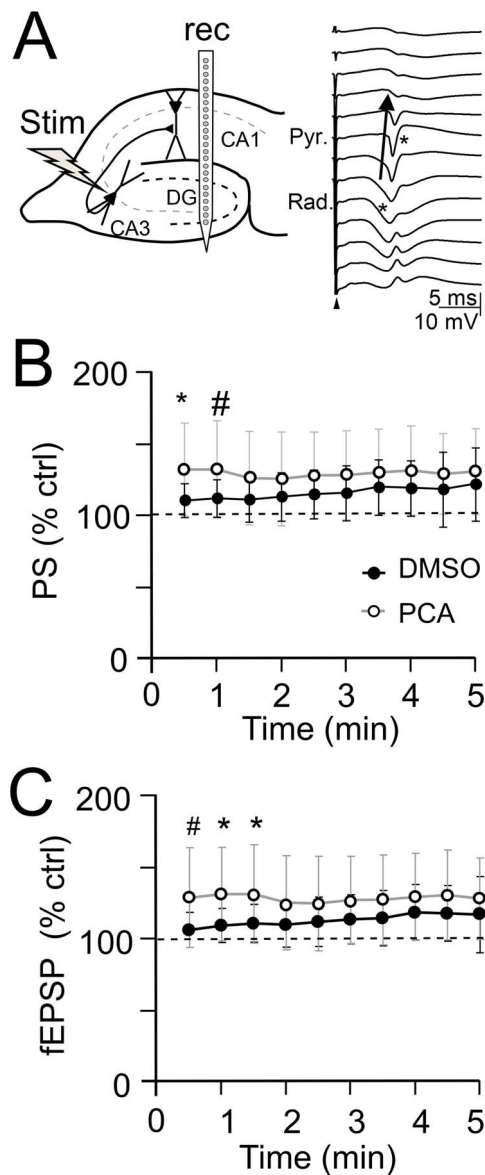


Fig. 3. Scheme of the electrode arrangement (A), and of the systemic (B,C) effects of PCA on CA1 evoked potentials. To explore the systemic effects of PCA, a linear array (rec) was used spanning the lower cortex, CA1 and DG. Stimuli were delivered to the CA3b for Schaffer activation (stim Schaffer). An evoked profile for supra-threshold activation is shown to the right. The fEPSP and PS were measured in optimal sites in the st. radiatum and pyramidal, respectively. The arrow indicated the forward conduction of the PS initiated in the st. radiatum. (B) The effects of a single intraperitoneal PCA injection on the o-PS (B) and f-EPSP (C). The stimulus intensity was set to obtain 30% of maximal PS response. The time points represent the mean \pm s.e.m. of $n = 6$ responses and as a control, the vehicle (DMSO) was injected in another group of animals. A mild increase of the two potentials was observed after PCA administration that reached a significant level in the first minutes. All the data are normalized to the corresponding pre-injection values: CTRL ($n = 5 \times 2$), ACSF ($n = 5 \times 2$), PCA ($n = 5 \times 2$).

Systemic delivery of PCA produces a lasting mild change to the spontaneous activity at specific FP generators

In light of the above, we explored if systemic delivery of PCA might produce persistent alterations to ongoing activity in the hippocampus and cortex by examining pathway-specific FP generators, these obtained from multisite spatial maps of FPs using

the ICA. FP generators avoid the mutual distortion of waveforms inherent to raw FPs and hence, drug-induced changes can be more accurately explored over time (Herreras et al. 2015). The site-dependency of raw (multisource) FPs recorded from the cortex (upper traces) down to the DG was analyzed, extracting FP generators through the ICA (Fig. 4, colored traces and profiles). There were differences between the waveforms and patterns of raw FPs, and those of the isolated FP generators, which were more prominent at some sites rather than others, reflecting each one's distinct power at different sites (see spatial voltage profiles at the top right panel). As such, we examined the following main FP generators identified through their characteristic profiles (Benito et al. 2014, 2016): the Schaffer input to CA1 (Sch); the input to the st. L-M in the CA1 (anatomical projections from the alvear tract, nucleus reuniens, and interneurons in the st. oriens all coincide in this stratum); the Perforant Path input from the entorhinal cortex to the DG (PP); an inhibitory input to granule cell somata (GCsom); and the main FP component in the cortex (Ctx).

The dynamics of the basal electrical activity were quite variable, similar to wakefulness but with dominant patterns characteristic of anesthesia. Slow-wave activity (SWA) dominated in the cortex and irregular activity interspersed with epochs of gamma, alpha, or beta oscillations in specific sub-fields and strata of the hippocampus (Hauer et al. 2022). In addition, some theta episodes occurred that generally presented in a discontinuous manner as bouts of varying duration (ranging 1 s to 1 min in different animals) and were highly conspicuous in the perirhinal recording sites. Theta activity was captured in L-M generator. In a still longer time scale, FP activity appeared as intermittent bursts of strong and weak power that lasted up to several minutes (Fig. 5A). The pattern and duration of these periods was heterogeneous between individuals, although the mean power was generator-specific and remained within fairly stable limits in each animal. The latter condition was considered the minimum stability criterion for validating drug effects. Since different FP patterns may appear in control conditions we used different quantification strategies to account for the multiple time scales in which FP activity develops, i.e. individual waves, patterns, and trends.

The compacted temporal displays of the power envelope ($\Delta t = 5$ s: Fig. 5A) for FP generators in individual animals already revealed gross changes in some of them after systemic i.p. injection of PCA. This means that at least some waves were larger than average after PCA injection (see below). Alterations appeared 2–5 min after injection; they peaked after 10–15 min and then faded over 30 min. In comparison to ACSF or DMSO injections, the PCA induced changes in one or several of the following: the regularity, duration, amplitude, temporal structure, or baseline level of activity. However, the population data was barely affected (Fig. 5B) due to large inter-animal variability and the prevalence of low frequency waves on this parameter (see below). Only one FP generator reached statistical significance (GCsom), although clear changes in other generators were observed in individuals.

Systemic PCA produces functional disengagement between cortical and hippocampal activities

Fig. 6A shows the active (synaptic) areas along the principal neurons in the cortex and hippocampus (Benito et al. 2014; Torres et al. 2019) to help envisioning the anatomo-functional relationships between them. Although in the short time scale the activity of different generators was highly discrepant (Fig. 4) they typically exhibited parallel changes of the level of activity in a scale of minutes, in which high and low power episodes appeared concerted in

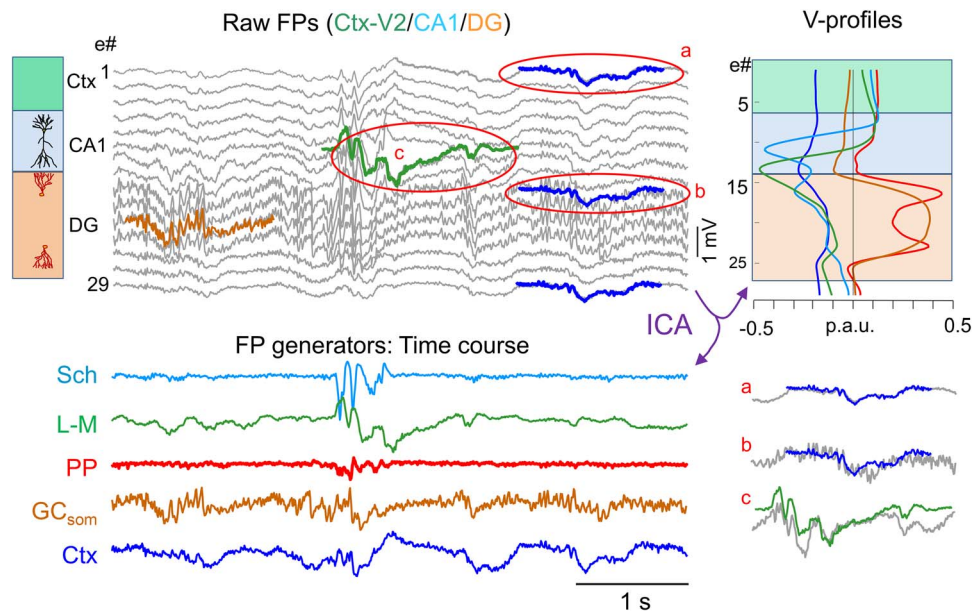


Fig. 4. Disentangling the FP generators to access the pathway-specific time courses. Sample epochs of raw FPs (upper traces in gray) recorded using a linear array across the V2 cortex and the CA1/DG (only every other channel is displayed), and showing the site-dependence and multifarious collection of FP waveforms. The ICA returns spatially coherent components (FP generators) and provides readout of the temporal dynamics free from the contribution of others (color-coded traces). The five main FP generators separated are labeled according to their maximal anatomical layers: Sch (CA1 Schaffer), L-M (CA1 st. lacunosum-moleculare), PP (perforant path input to DG), GC_{som} (somatic input to granule cells), and Ctx (main cortical generator). The amplitudes are presented in proportional arbitrary units and the corresponding spatial distribution (i.e. the relative power along the recording track) is shown on the right (voltage [V]-profiles). A few instances are superimposed onto the raw FPs to facilitate their visual matching/unmatching. The better the FP generator matches the raw FP at a particular recording site, the larger its relative contribution, as illustrated by the parts of the recordings highlighted by red ovals and extracted below: (a) a slow wave in the Ctx generator (dark blue) tightly matches the raw FPs in upper (cortical) channels (in gray), but it also spreads by volume conduction all the way down to the DG (b), where it accounts for the slow envelope of the FP there, although at this site there are also faster superimposed oscillations generated at other sites. This justifies the use of FP generators as opposed to raw FPs to quantify electrical activity: E#, electrode number: Only every other channel is displayed.

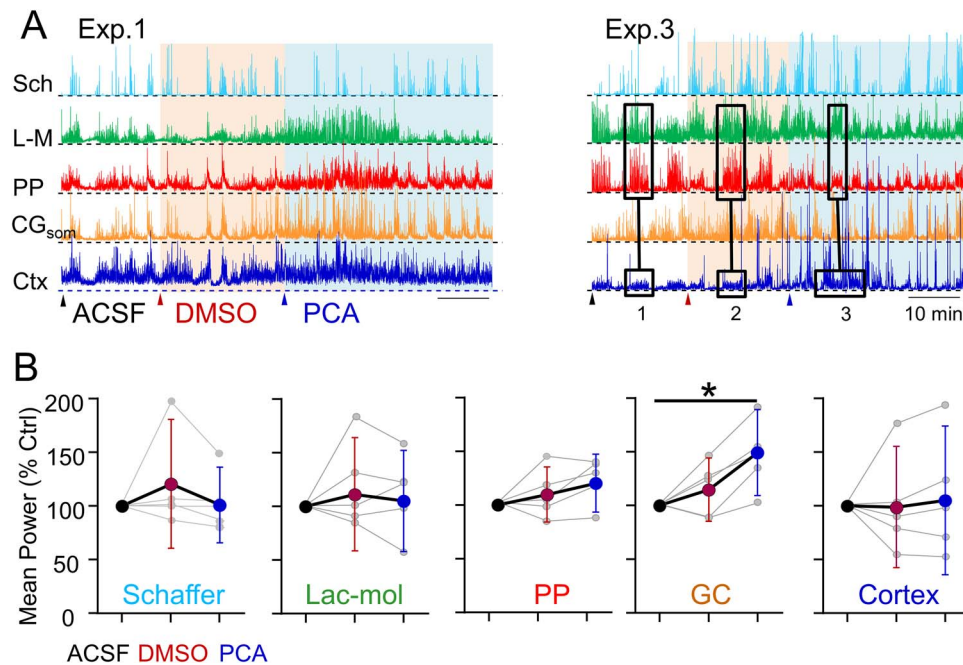


Fig. 5. PCA has a variable mild effect on the ongoing activity of separated FP generators. (A) Time plots of the power of the separate FP generators in two experiments (vertical scale is in normalized arbitrary units). The sliding time window is 1 s. Time-compact plots are generated maintaining local maxima. The colored backgrounds mark the periods after each injection (arrowheads). Although the resting patterns of activity (ACSF and DMSO) could differ among animals, there is clearly tight covariance between the cortical and hippocampal generators (except the Schaffer). Note the graded and selective action of PCA on some generators and the disruption of cortico-hippocampal covariance. The epochs marked by the black boxes 2 and 3 are amplified in Fig. 6. (B) Mean power and standard error for each FP generator evaluated over epochs of 15 mins after each injection. The values from individual animals are in gray and the data are normalized with respect to the ACSF ($n=6$; ANOVA plus Bonferroni post-hoc test).

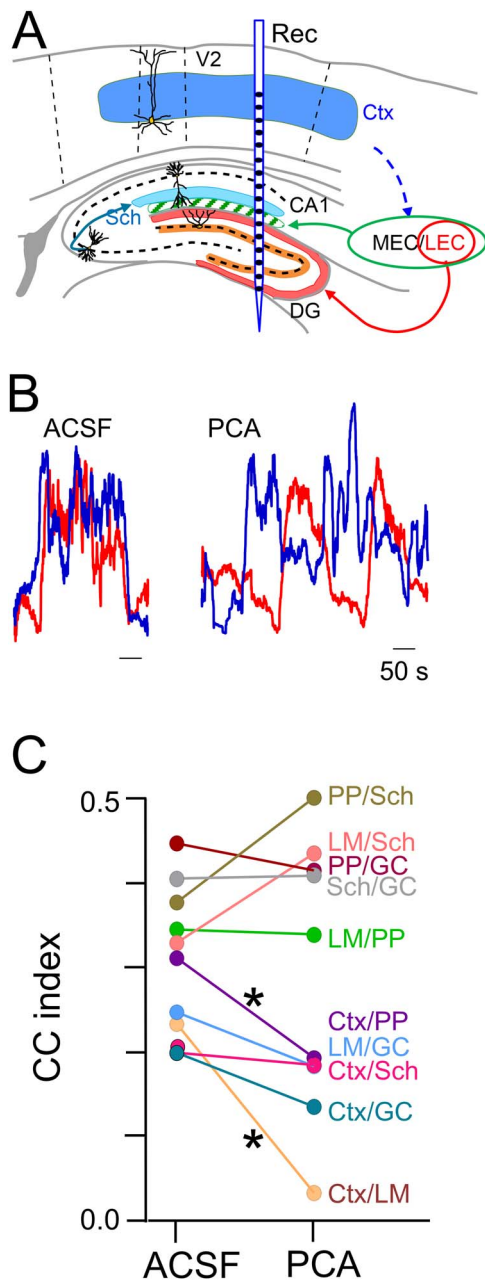


Fig. 6. PCA produces cortico-hippocampal disengagement. (A) Drawing of a sagittal section taken from the rat brain atlas on which the active (synaptic) zones of the FP generators whose ongoing activity has been cross-correlated. Color codes as in previous figures. Some of the relevant connections have been signaled by arrows. MEC/LEC: Medial and lateral entorhinal cortices. V2: Visual cortex. (B) Enlargement of segments marked in Fig. 5B (boxes 2 and 3) for the activity in the PP (red) and cortical (blue) FP generators, before (ACSF) and after i.p. PCA delivery. (C) Pair-wise CC index between all FP generators. Note that PCA induced a drop of correlation between the cortical and all but the Sch hippocampal generators (student t-test, $n = 5$).

both structures (Fig. 5A, ACSF). Such strong correlation was maintained after DMSO administration (Fig. 5A, Exp#3, boxes 1 and 2). However, i.p. delivery of PCA disrupted this temporal relationship between the generators of different structures (Fig. 5A, box 3, and enlargements in Fig. 6B), i.e. between those in the hippocampus and the main generator of the cortex. Conversely, the correlation remained strong internally among the hippocampal sub-fields and generators. The cross-correlation (CC) index between power

envelopes for pairs of generators confirmed this (Fig. 6C). For instance, the mean CC between Ctx and L-M FP generators was 0.23 ± 0.06 after ACSF administration but it dropped to 0.03 ± 0.05 after PCA delivery ($t = 6.56$, $P = 0.001$; Student t-test, $n = 5$ animals), whereas the CC between L-M and PP FP generators was 0.35 ± 0.11 after ACSF (ctrl) and 0.34 ± 0.14 after PCA ($t = 0.07$, $P = 0.47$). Hence, PCA produced functional detachment between the FP activities in the cortex and hippocampus.

Heterogeneous effects of systemic PCA on different parameters of FP generators at short timescales

We then explored whether the effects of PCA on minute-scale co-modulation of hippocampal and cortical activities had any counterpart in commonly assessed short-term scale parameters. First, we examined the effect of PCA on the frequency content of specific FP generators. Significant alterations of specific frequency bands after systemic PCA were found in 10 of the 25 possible pair-wise comparisons (five generators and five frequency bands: Supplementary Fig. 1). These were mainly found in the L-M, GCsom, and PP generators of the hippocampus, and within medium-high frequency bands (theta and beta), although some generators were also altered in the alpha and gamma bands. In all of these, the mean power increased after PCA delivery. Notably, an increase in the mean power was also evident after DMSO administration in four comparisons. The cortical FP generator was barely altered in any frequency band and it also presented the weakest population variability. A dominant contribution of low frequencies (SWA) to the overall power (Fig. 5B) may explain the failure to reveal population effects in this case.

We also explored the effects of PCA on the number of waves per unit time in each FP generator by setting a series of voltage thresholds (in times the standard deviation: $0.5x\sigma$, σ , $2x\sigma$, and $3x\sigma$). An illustrative example for the Sch and L-M generators in a representative animal is shown in Fig. 7A and B, respectively. The PCA transiently modified the number of waves per second in some FP generators (epochs shaded in gray), an effect that was unmasked as the threshold for detection increased. However, these observations were not clearly appreciated in the population analysis due to inter-animal variability. Only one generator returned a slight non-significant difference (PP generator at $\sigma = 1$, $P = 0.016$, $U = 24$; Mann-Whitney test followed by Bonferroni). Since fast small-amplitude waves may not be detected when riding on slow ones, we repeated the analysis after splitting the time course of the FP generator into two frequency bands above and below 10 Hz. Thus, one contained mostly delta and theta activity, while the other was predominantly in the beta, alpha, and gamma bands. This procedure optimized the counting of the waves, and some differences in the effect of PCA were readily appreciated in certain individuals (Supplementary Fig. 2). However, the population statistics rendered similar results as the wideband analysis.

Lastly, we investigated the potential effects of drug treatment on the density distributions of time values for each FP generator. This analysis was motivated by the consideration that substantial spatiotemporal overlap of waves generated by co-active sources can lead to the emergence of spurious frequencies in mesoscopic FPs, which may introduce biases when using Fourier methods for characterization. In contrast, analyzing baseline voltage fluctuations might better capture fine-grained dynamics. To achieve this, we calculated the mean, standard deviation, kurtosis, and skewness of the voltage distributions for each generator. We assessed

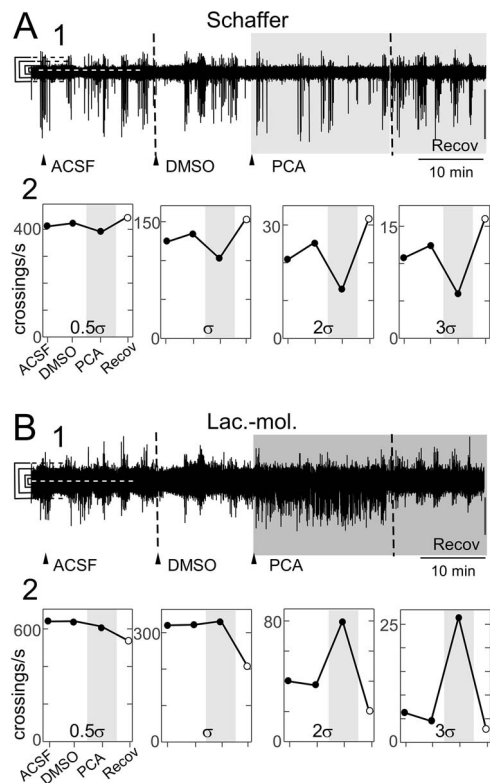


Fig. 7. The effects of PCA on the number of waves in FP generators at different voltage thresholds. The mean value is indicated by the white dashed line, and the thresholds are indicated to the left as 0.5, 1, 2, and 3 times the value of the standard deviation of the mean. (A), (B) correspond to the Schaffer and lac-Mol generators in the same animal, respectively. The upper traces (A1, B1) show the time course of the activity over a compact scale. The number of waves per second is plotted below (A2, B2) for each voltage threshold. The voltage in the FP generators was estimated at the site that presented the maxima. At the Schaffer generator, the bulk of the waves belong to small amplitude (50–200 μ V) gamma waves contained in the thick baseline, whereas the large strokes belong to sharp-wave complexes. In the L-M generator, the duration of the waves had a greater dispersion, giving a more irregular global pattern. The longer waves induced by PCA were mostly delta-type slow waves.

the potential bias arising from spontaneous changes in the electrographic state (presence or absence of theta) during the different treatments. It's worth to note that theta activity occurred rarely at the anesthetic level utilized in our study, manifesting as short-lasting bouts of weak power (Fig. 8A). Although theta predominantly appeared in the L-M generator, associated changes in the fine temporal structure might exist in other generators. To explore this, we examined possible theta-related alterations in the distributions of all generators through the Pearson correlation. The mean theta power was estimated for each of the 50 consecutive epochs, with each epoch spanning 90 s, and we segmented the time course of each generator (including all treatments) accordingly (Fig. 8A, lower plot). Due to significant statistical differences between homonymous generators in different animals (Fig. 8B), we normalized the values for each parameter in each generator and treatment across all individuals (Fig. 8C). This normalization allowed us to account for individual variability and improve the robustness of our analyses.

We observed minimal effects of the presence or absence of theta on the distribution parameters for all generators (refer to statistics in Supplementary Table 1). Only the skewness of the L-M generator showed correlation coefficients close to -0.5 , while

most others scored below ± 0.2 . Subsequently, we focused on examining the effects of PCA compared to the period immediately preceding it, following DMSO injection. Individual results exhibited variations across different generators (see Fig. 8D), prompting us to pool all normalized values for each parameter across the animal population to obtain global statistics. Overall, PCA induced significant changes in 8 out of 20 parameters (five generators with four parameters each), with notable effects in the generators of the DG (LPP and GCsom) (Supplementary Table 2). The parameters most frequently affected were the mean and the skewness, each showing changes in three out of five generators. These findings highlight the specific impact of PCA on certain distribution parameters and provide further insights into its effects on the generators' dynamics.

Discussion

The present study shows that the phenolic compound PCA alters electrophysiological activity in the hippocampus. We report an increase of spike threshold (rheobase) ex vivo and reduced or no effect of synaptic firing ex vivo and in vivo, respectively, as well as mild effects on the ongoing activity of some pathway-specific FP generators. Notably, we found a detachment of overall cortico-hippocampal coherence in long-time scales. To our knowledge, this is the first report showing direct action of a dietary polyphenol on electrical activity of neurons and circuits. Accordingly, we propose that some polyphenols may exert a direct neuromodulatory-like action on central brain structures.

Whereas the single cell electrophysiology of CA1 pyramidal cells ex vivo is well known, the use of raw FPs has a number of caveats derived from the multisource and spatial nature of these signals (Herreras 2016; Herreras et al. 2022). Here, we minimized these by using an ICA that extracts spatially coherent components or FP generators (Makarov et al. 2010; Głabaska et al. 2014). This step provides more realistic time courses by avoiding mutual contamination between spatially overlapped sources or with potentials originated in distant sources (volume conduction), both of which affect measurements like the mean power or the frequency content, as well as correlations between activities in different sites (Herreras 2016; Torres et al. 2019). The spatial gradients and landmarks of the FP generators obtained in this study were those reported previously, which helped the identification of the synaptic pathways promoting the currents that give raise to FP generators (Benito et al. 2014, 2016).

On the other hand, the FP analysis presented here highlights the difficulties in characterizing/quantifying ongoing population activities, particularly in absence of stimuli or events that can be timed to waves or patterns that enable averaging. We are not aware of effective ways to achieve inter-animal normalization of spontaneous FP activity in central structures of anesthetized animals without severely limiting the repertoire of electrographic states. Some attempts to use entropy are being essayed (Li et al. 2016), but still require maturation before a reliable physiological interpretation is obtained. The FP-generators employed here proved useful in this respect. Admittedly, we might have optimized this by using a deeper anesthetic plane to achieve a more stable and uniform electrographic pattern (Torao-Angosto et al. 2021). However, we chose to collect data as close as possible to FPs in awoken animals so as not to limit the potential utility of the study.

In relation to this, it comes clear a stronger benefit of FP generators to reveal correlated changes over long-time scales rather than to unveil possible changes on the short-term features of FP

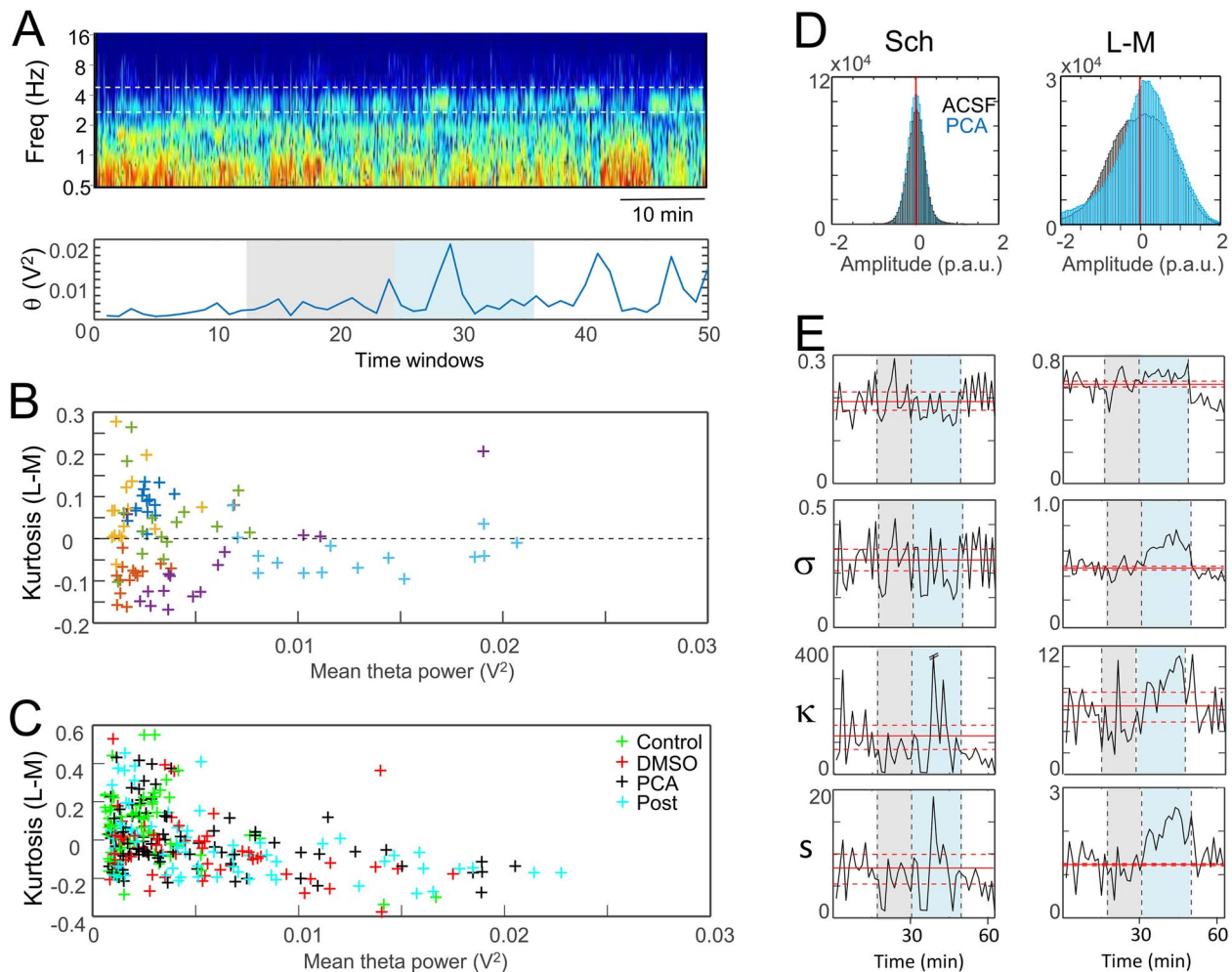


Fig. 8. Density distributions of the time-point voltages efficiently unmasks the effects of PCA on the time course of FP generators. The parameters analyzed were the mean (\bar{x}), standard deviation (σ), kurtosis (κ), and the skewness (s). (A) In order to anticipate for possible changes of the fine-grained dynamics during spontaneous occurrence of theta episodes these were quantified as the mean power in the theta band (3.5–5 Hz: White dashed lines in wavelet spectrum) of the theta-bearing L-M generator in fifty windows spanning all treatments (lower plot). (B) Variability of the distribution parameters for a specific generator among the population. As an example, the plot illustrates the values for the kurtosis in the L-M generator after PCA injection in all animals in function of the theta power in the corresponding window. Each animal is coded by a different color. This particular example scored among the highest correlations with ongoing theta power, which were generally negligible (Supplementary Table 1). (C) The distributions in different animals and generators were normalized (mean and standard deviation) to enable population statistics among the different treatments. (D) The left and right plots show a representative example of the superimposed distributions of time point voltages after ACSF and PCA injections in one animal for the Schaffer and lac-Mol generators. (E) The epochs were split into consecutive 90 s fragments and the distribution parameters plotted as successive values (black lines). The mean and 95% confident limits were estimated for the control period and are represented by horizontal red lines expanded to all treatments to facilitate the visual comparison. In the example illustrated, the values characterizing the distribution for the Schaffer generator were about the same in DMSO and PCA (gray and blue shadows), whereas PCA modified the standard deviation and the skewness for the lac-Mol generator. See population statistics in Supplementary Table 2.

activity upon treatments with compounds as the PCA involved in slow-developing phenomena. Indeed, despite the strong overall coherence of activity levels in the long-time scale across the cortex and hippocampus the diversity and unpredictable duration of the multiple motifs and oscillations developing on shorter time scales leads to large inter-animal dispersion that strongly affects population statistics evaluated on short-term parameters, despite of significant within-animal effects of the drug. Admittedly, individual FP waves and short FP motifs are shaped by synchronous firing on cell assemblies and paced by local networks, respectively (Traub et al. 1999; Mazzoni et al. 2010; Fernández-Ruiz et al. 2012; Herreras et al. 2022). The mechanisms underlying this global coherence between structures probably overpass the capabilities of pacemakers and clocking phenomena that set standard network oscillations. Varying levels of activity on the scale of

minutes to hours are more related to functional states, which are governed by neuromodulatory agents (Lee and Dan 2012; Nadim and Bucher 2014). We have previously successfully used FP generators to reveal ongoing changes in Schaffer FP activity for days after spinogenic treatment (Enriquez-Barreto et al. 2014), but this also affected the amplitude of individual Schaffer gamma waves (hence the mean power), which is not the case when using the polyphenol PCA.

The cellular actions of PCA appear to target intrinsic properties

While the limited action of PCA on the EPSP amplitude in the Schaffer pathway in single cells ex vivo is consistent with the population response in vivo, the significant increase of EPSPs in basal dendrites ex vivo could potentially indicate facilitated

synaptic transmission in specific synapses. This effect may be attributed to PCA's impact on astrocyte glutamate transporters, modifying their ability to remove glutamate from the synaptic cleft and, consequently, influencing the time course of EPSPs (Bergles and Jahr 1998). Previous studies have reported differences between basal and apical excitatory synapses (Mattison et al. 2014; Brzdak et al. 2019). In both basal and apical dendrites, the EPSPs are noticeably elongated by PCA, while the initial slope is minimally affected. However, if synaptic transmission were facilitated, one would also expect an increase in the initial slope. The elongation of EPSPs might also be attributed to an effect on the kinetics of synaptic receptors (Marcaggi et al. 2009). However, other data from this study suggest a postsynaptic mechanism, as evidenced by the failure to repolarize the membrane upon synaptic depolarization (Hoffman et al. 1997). The pronounced increase in peak amplitude specific to basal dendrites could be explained by a similar mechanism. These dendrites are thinner and more electrically compact than apical dendrites, allowing even a slight down-modulation of repolarizing channels to release the full depolarizing power of glutamate receptors earlier and more efficiently compared to the thicker and longer apical shaft, which requires more current and longer charging times. Alternatively, an enhancement of intrinsic depolarizing Na⁺ and Ca⁺⁺ channels may lead to similar observations, as these channels are known to amplify EPSPs (Lipowsky et al. 1996; Canals et al. 2005).

Additional results indicate that PCA exerts further effects on the intrinsic properties of these neurons. Specifically, cell firing was significantly reduced in response to both synaptic input and depolarizing currents injected at the soma. These observations suggest domain-specific actions, likely resulting from the heterogeneous distribution of intrinsic channels along the somatodendritic body (Johnston et al. 2000). Although there was no significant change in the somatic spike waveform during PCA, one plausible explanation for the blockade of cell firing is that PCA destabilizes membranes at distant sites with a high density of Na⁺ channels, such as the axon hillock (Hamdan et al. 2020).

Thus, in juvenile rats *ex vivo*, the spike nearly always initiates there and invades the soma and dendrite retrogradely (Miyakawa and Kato 1986; Canals et al. 2005). This highly specialized membrane may fail to initiate spikes for instance if PCA destabilizes this protein-rich membrane area and anchoring protein re-assembly is required. The possibility of increased rheobase and voltage threshold during PCA aligns with the findings of this study. Interestingly, the maintenance of synaptically evoked PS after systemic administration of PCA *in vivo* is not contradicted by its strong spike depressant activity observed *ex vivo*. *In vivo* experiments consistently demonstrate that supra-threshold evoked potentials elicit spikes in the apical trunk, which then propagate forward to the soma (Herreras 1990; Kloosterman et al. 2001; see also Fig. 3). Invasion of the soma by an apically initiated spike may occur without the direct involvement of the axon hillock (Ibarz et al. 2006), which may or may not fire later depending on whether it was selectively interfered with, for instance, by PCA. The reduced rising slope of somatic spikes during PCA is consistent with a decreased electrotonic contribution of putative spikes originating from the axon hillock (López-Aguado et al. 2002).

Without additional information, the opposite behavior of PCA on synaptic responses and cell firing may have several explanations, such as differences in the concentration of PCA that reaches the target site depending on the route of administration, or the multiplicity of actions at different cellular targets. Similar neuromodulatory-like actions of orthodromic responses

have been observed for various neuroactive compounds, such as activators of the corticotropin-releasing hormone type 1 receptor and P2 purinergic receptors, or some protein kinase C inhibitors (Corradetti et al. 1989; Coppi et al. 2007; Kratzer et al. 2013). As such, future studies should address whether the effects of PCA on hippocampal excitatory transmission interact with these or other receptors/signaling pathways. It is important to note that a small or even null effect on evoked potentials does not rule out changes in the ongoing activity in the pathway stimulated (see below).

Some reported effects of PCA, such as its antioxidant properties (Zhang et al. 2021), may play such a role altering the physicochemical properties of the membrane or the extracellular matrix. It will also be important to explore the range of effective concentrations of PCA in order to establish appropriate ranges for any beneficial/detrimental effects of this compound (Song et al. 2020).

Cortico-hippocampal disengagement by PCA

Overall, the systemic effects of PCA are relatively mild, and concerning the FP generators, they display some degree of instability. However, despite these limitations, a robust finding in this study, supported by population statistics, is the PCA-induced decrease in the CC between the cortical and hippocampal FP generators, while the CC between hippocampal subpopulations is not affected. In principle, this observation suggests a functional disengagement between the cortex and hippocampus. Since FPs are convolutions of synaptic activity it might be argued that some of these hippocampal generators (e.g. the PP generator, and partially also the L-M) also reflect cortical (entorhinal) input, in which case such disengagement would be better defined as cortico-cortical, i.e. among different cortical areas. This result aligns with the main effect of PCA on the distribution parameters of the DG generators, whose dynamics reflect the input received from the lateral entorhinal cortex. Indeed, it is known that SWA in the cortex spreads across cortical areas although some regions may be sidelined (Pazienti et al. 2022). In unpublished results in anesthetized rats, we observed SWA in the somatosensory cortex that did not spread to the entorhinal cortex, which could be displaying faster FPs, including theta. A reduction of the overall cortico-hippocampal CC index may arise after changes to the dominant electrographic pattern, shifting from that based on delta activity to another based on fast activity. One such change characterizes the transition from sleep to awakening (Steriade et al. 2001). Although occasional epochs of theta activity were observed in these experiments, they were short-lasting, intermittent, and exhibited weak regularity. Furthermore, we ensured that these theta epochs did not significantly impact the overall statistics of PCA effects. A similar reaction can also be achieved through enhanced sensitivity to brainstem inputs, which are known to be modulated by polyphenols (Ates et al. 2007; Revuelta et al. 2016). In some individuals we saw an intermittent transition from SWA in the control toward a desynchronized state after PCA delivery, although this could not be generalized due to the variation in the resting patterns among the population.

In the present study we addressed the acute electrophysiological effects of PCA administered in a single-dose protocol, observing effects lasting from a few to tens of minutes. However, the literature available reports the long-term benefits of PCA due to possible antioxidant, anti-inflammatory (Lee et al. 2018), immunoregulatory (Anderson et al. 2020) and even neuroprotective effects (Krzysztoforska et al. 2019). In this context, our results should be taken with caution, and the effects of PCA on additional

cerebral and systemic targets should be explored over different time scales.

In relation to this, infraslow brain activity is reminiscent of the resting state fluctuations reported in humans (Drew et al. 2008; Lőrincz et al. 2009; Picchioni et al. 2011), although the underlying mechanisms are as yet poorly understood. In animal models, some ultraslow potentials are related to glial-mediated network synchronization (Hughes et al. 2011). Indeed, it would be interesting to check the effects of polyphenols on glial cells, since PCA is known to produce multiple neuroprotective effects in some pathologies. For instance, PCA decreases the levels of oxidative stress (Al Olayan et al. 2020; Gao et al. 2020) and neuroinflammation (Lin et al. 2009; Min et al. 2010), events in which glia are known to have a primary role (Largo et al. 1996). Interestingly, both astrocytes and microglial cells are known to express a variety of membrane channels similar to those responsible for intrinsic properties in neurons (Schmaul et al. 2021; Sarkar 2022; Wang et al. 2022).

Concluding remarks

This study shows that PCA directly targets the hippocampus, and that it has both acute and sustained actions on cell and network electrophysiology, as well as on global coherence between structures. Some of the results point to specific effects on intrinsic membrane properties and thus, we suggest future studies should also investigate the actions of polyphenols on different structures as well as on cells other than neurons. Nonspecific non-neuronal effects make it likely that polyphenols could interact synergistically with individual or environmental conditions, such as the animal's metabolic state or genetic factors. We take the present results as evidence for the direct effects of a dietary polyphenol on the electrical activity of neurons, which is compatible with reported actions on cell signaling routes since both are tightly interdependent (Hong et al. 2005; Flavell et al. 2006). Integration of cellular and electrical data would seem an obvious goal for understanding the physiological and pathological processes involved in long-lasting, experience-dependent changes in the nervous system that occur on scales of hours to years, and how best to use diet-derived compounds or other drugs for medical purposes.

Acknowledgments

We thank Mark Sefton at BiomedRed for editorial assistance. OH and JM belong to the Cajal Blue Brain Interdisciplinary Platform of the CSIC, Spain.

Author contributions

Marta Montero-Atalaya (Data curation, Investigation), Sara Expósito (Data curation, Formal analysis, Investigation, Methodology, Writing—review & editing), Ricardo Muñoz-Arnaiz (Data curation, Formal analysis), Julia Makarova (Data curation, Methodology, Supervision), Begoña Bartolomé (Supervision, Writing—review & editing), Eduardo Martín (Formal analysis, Funding acquisition, Methodology, Resources, Writing—original draft), M. Victoria Moreno-Arribas (Conceptualization, Funding acquisition, Methodology, Resources, Writing—review & editing), and Oscar Herreras (Conceptualization, Formal analysis, Funding acquisition, Methodology, Project administration, Resources, Supervision, Writing—original draft, Writing—review & editing)

Supplementary material

Supplementary material is available at *Cerebral Cortex* online.

Funding

This work was supported by the Spanish Ministerio de Ciencia e Innovación (OH, PID2019-111587RB-I00, EM, PID2020-116327GB-I00; MVMA and BB, PID2019-108851RB-C21; and MM, PRE2020-093312) and by the Agencia Estatal de Evaluación, Next Generation EU grant (PDC2021-121103-I00) to OH.

Conflict of interest statement: None declared.

References

- Al Olayan EM, Aloufi AS, AlAmri OD, el-Habit OH, Abdel Moneim AE. Protocatechuic acid mitigates cadmium-induced neurotoxicity in rats: role of oxidative stress, inflammation and apoptosis. *Sci Total Environ.* 2020;723:137969.
- Anderson K, Ryan N, Siddiqui A, Pero T, Volpedo G, Cooperstone JL, Oghumu S. Black raspberries and protocatechuic acid mitigate dnfβ-induced contact hypersensitivity by down-regulating dendritic cell activation and inhibiting mediators of effector responses. *Nutrients.* 2020;12(6):1701.
- Ates O, Cayli SR, Yucel N, Altinoz E, Kocak A, Durak MA, Turkoz Y, Yologlu S. Central nervous system protection by resveratrol in streptozotocin-induced diabetic rats. *J Clin Neurosci.* 2007;14(3):256–260.
- Bell A, Sejnowski T. An information-maximization approach to blind separation and blind deconvolution. *Neural Comput.* 1995;7(6):1129–1159.
- Benito N, Fernández-Ruiz A, Makarov VA, Makarova J, Korovaichuk A, Herreras O. Spatial modules of coherent activity in pathway-specific LFPs in the hippocampus reflect topology and different modes of presynaptic synchronization. *Cereb Cortex.* 2014;24(7):1738–1752.
- Benito N, Martín-Vázquez G, Makarova J, Makarov VA, Herreras O. The right hippocampus leads the bilateral integration of gamma-parsed lateralized information. *Elife.* 2016;5:e16658.
- Bergles DE, Jahr CE. Glial contribution to glutamate uptake at Schaffer collateral-commissural synapses in the hippocampus. *J Neurosci.* 1998;18(19):7709–7716.
- Brdzak P, Wójcicka O, Zareba-Kozioł M, Minge D, Henneberger C, Włodarczyk J, Mozzymas JW, Wójtowicz T. Synaptic potentiation at basal and apical dendrites of hippocampal pyramidal neurons involves activation of a distinct set of extracellular and intracellular molecular cues. *Cereb Cortex.* 2019;29(1):283–304.
- Canals S, López-Aguado L, Herreras O. Synaptically-recruited apical currents are required to initiate axonal and apical spikes in hippocampal pyramidal cells: modulation by inhibition. *J Neurophysiol.* 2005;93(2):909–918.
- Carecho R, Carregosa D, dos Santos CN. Low molecular weight (poly)phenol metabolites across the blood-brain barrier: the underexplored journey. *Brain Plast.* 2021;6(2):193–214.
- Carregosa D, Mota S, Ferreira S, Alves-Dias B, Loncarevic-Vasiljkovic N, Crespo CL, Menezes R, Teodoro R, Santos CND. Overview of beneficial effects of (poly)phenol metabolites in the context of neurodegenerative diseases on model organisms. *Nutrients.* 2021;13(9):2940.
- Chen A. Fast kernel density independent component analysis. *Lecture Notes Comput Sci.* 2006;3889:24–31.

- Coppi E, Pugliese AM, Stephan H, Müller CE, Pedata F. Role of P2 purinergic receptors in synaptic transmission under normoxic and ischaemic conditions in the CA1 region of rat hippocampal slices. *Purinergic Signal*. 2007;3(3):203–219.
- Corradetti R, Pugliese AM, Ropert N. The protein kinase C inhibitor 1-(5-isoquinolinesulphonyl)-2-methylpiperazine (H-7) disinhibits CA1 pyramidal cells in rat hippocampal slices. *British J Pharmacol*. 1989;98(4):1376–1382.
- Cueva C, Gil-Sánchez I, Ayuda-Durán B, González-Manzano S, González-Paramás A, Santos-Buelga C, Bartolomé B, Moreno-Arribas M, Moreno-Arribas MV. An integrated view of the effects of grape and wine polyphenols and their relevant metabolites on gut and host health. *Molecules*. 2017;22(1):99.
- Drew PJ, Duyn JH, Golanov E, Kleinfeld D. Finding coherence in spontaneous oscillations. *Nat Neurosci*. 2008;11(9):991–993.
- Enríquez-Barreto L, Cuesto G, Domínguez-Iturza N, Gavilán E, Ruano D, Sandi C, Fernández-Ruiz A, Martín-Vázquez G, Herreras O, Morales M. Learning improvement after PI3K activation correlates with de novo formation of functional small spines. *Front Mol Neurosci*. 2014;6:54.
- Fernández M, Lao-Peregrín C, Martín ED. Flufenamic acid suppresses epileptiform activity in hippocampus by reducing excitatory synaptic transmission and neuronal excitability. *Epilepsia*. 2010;51(3):384–390.
- Fernández-Ruiz A, Makarov VA, Benito N, Herreras O. Schaffer-specific local field potentials reflect discrete excitatory events at gamma-frequency that may fire postsynaptic hippocampal CA1 units. *J Neurosci*. 2012;32(15):5165–5176.
- Figueira I, Garcia G, Pimpão RC, Terrasso AP, Costa I, Almeida AF, Tavares L, Pais TF, Pinto P, Ventura MR, et al. Polyphenols journey through blood-brain barrier towards neuronal protection. *Sci Rep*. 2017;7(1):11456.
- Figueira I, Tavares L, Jardim C, Costa I, Terrasso AP, Almeida AF, Govers C, Mes JJ, Gardner R, Becker JD, et al. Blood-brain barrier transport and neuroprotective potential of blackberry-digested polyphenols: an in vitro study. *Eur J Nutr*. 2019;58(1):113–130.
- Flavell SW, Cowan CW, Kim T-K, Greer PL, Lin Y, Paradis S, Griffith EC, Hu LS, Chen C, Greenberg ME. Activity-dependent regulation of MEF2 transcription factors suppresses excitatory synapse number. *Science*. 2006;311(5763):1008–1012.
- Gao Y, Ma L, Han T, Wang M, Zhang D, Wang Y. Protective role of protocatechuic acid in sevoflurane-induced neuron apoptosis, inflammation and oxidative stress in mice. *Restor Neurol Neurosci*. 2020;38(4):323–331.
- Gasperotti M, Passamonti S, Tramer F, Masuero D, Guella G, Mattivi F, Vrhovsek U. Fate of microbial metabolites of dietary polyphenols in rats: is the brain their target destination? *ACS Chem Neurosci*. 2015;6(8):1341–1352.
- Głąbska H, Potworowski J, Łęski S, Wójcik DK. Independent components of neural activity carry information on individual populations. *PLoS One*. 2014;9(8):e105071.
- Hajipour S, Sarkaki A, Farbood Y, Eidi A, Mortazavi P, Valizadeh Z. Effect of gallic acid on dementia type of Alzheimer disease in rats: electrophysiological and histological studies. *Basic Clin Neurosci*. 2016;7(2):97–106.
- Hamdan H, Lim BC, Torii T, Joshi A, Konning M, Smith C, Palmer DJ, Ng P, Leterrier C, Osés-Prieto JA, et al. Mapping axon initial segment structure and function by multiplexed proximity biotinylation. *Nat Commun*. 2020;11(1):100.
- Hauer BE, Pagliardini S, Dickson CT. Tonic excitation of nucleus reuniens decreases prefrontal-hippocampal coordination during slow-wave states. *Hippocampus*. 2022;32(6):466–477.
- Helmich RC, Toni I, Deuschl G, Bloem BR. The pathophysiology of essential tremor and Parkinson's tremor. *Curr Neurol Neurosci Rep*. 2013;13(9):378.
- Herreras O. Propagating dendritic action potential mediates synaptic transmission in CA1 pyramidal cells in situ. *J Neurophysiol*. 1990;64(5):1429–1441.
- Herreras O. Local field potentials: myths and misunderstandings. *Front Neur Circuits*. 2016;10:101.
- Herreras O, Makarova J, Makarov VA. New uses of LFPs: pathway-specific threads obtained through spatial discrimination. *Neuroscience*. 2015;310:486–503.
- Herreras O, Torres D, Martín-Vázquez G, Hernández-Recio S, López-Madrona VJ, Benito N, Makarov VA, Makarova J. Site-dependent shaping of field potential waveforms. *Cereb Cortex*. 2022;2022:bhac297. <https://doi.org/10.1093/cercor/bhac297>.
- Ho L, Ferruzzi MG, Janle EM, Wang J, Gong B, Chen TY, Lobo J, Cooper B, Wu QL, Talcott ST, et al. Identification of brain-targeted bioactive dietary quercetin-3-O-glucuronide as a novel intervention for Alzheimer's disease. *FASEB J*. 2013;27(2):769–781.
- Hoffman DA, Magee JC, Colbert CM, Johnston D. K⁺ channel regulation of signal propagation in dendrites of hippocampal pyramidal neurons. *Nature*. 1997;387(6636):869–875.
- Hong EJ, McCord AE, Greenberg ME. A biological function for the neuronal activity-dependent component of Bdnf transcription in the development of cortical inhibition. *Neuron*. 2005;60(4):610–624.
- Hughes SW, Lorincz ML, Parri HR, Crunelli V. Infralow (<0.1 Hz) oscillations in thalamic relay nuclei basic mechanisms and significance to health and disease states. *Prog Brain Res*. 2011;193:145–162.
- Ibarz JM, Makarova I, Herreras O. Relation of apical dendritic spikes to output decision in CA1 pyramidal cells during synchronous activation: a computational study. *European Journal of Neuroscience*. 2006;23(5):1219–1233. <https://doi.org/10.1111/j.1460-9568.2006.04615.x>.
- Johnston D, Hoffman DA, Magee JC, Poolos NP, Watanabe S, Colbert CM, Migliore M. Dendritic potassium channels in hippocampal pyramidal neurons. *J Physiol*. 2000;525(1):75–81.
- Kale S, Sarode LP, Kharat A, Ambulkar S, Prakash A, Sakharkar AJ, Ugale RR. Protocatechuic acid prevents early hour ischemic reperfusion brain damage by restoring imbalance of neuronal cell death and survival proteins. *J Stroke Cerebrovasc Dis*. 2021;30(2):105507.
- Khan AK, Rashid R, Fatima N, Mahmood S, Mir S, Khan S, Jabeen N, Murtaza G. Pharmacological activities of protocatechuic acid. *Acta Pol Pharm*. 2015;72(4):643–650.
- Kim KJ, Hwang ES, Kim MJ, Rha CS, Song MC, Maeng S, Park JH, Kim DO. Effects of phenolic-rich *Pinus densiflora* extract on learning, memory, and hippocampal long-term potentiation in scopolamine-induced amnesic rats. *Antioxidants*. 2022;11(12):2497.
- Kloosterman F, Peloquin P, Leung LS. Apical and basal orthodromic population spikes in hippocampal CA1 in vivo show different origins and patterns of propagation. *J Neurophysiol*. 2001;86(5):2435–2444.
- Korovaichuk A, Makarova J, Makarov VA, Benito N, Herreras O. Minor contribution of principal excitatory pathways to hippocampal LFPs in the anesthetized rat: a combined independent component and current source density study. *J Neurophysiol*. 2010;104(1):484–497.
- Kratzer S, Mattusch C, Metzger MW, Dedic N, Noll-Hussong M, Kafitz KW, Eder M, Deussing JM, Holsboer F, Kochs E, et al. Activation of CRH receptor type 1 expressed on glutamatergic

- neurons increases excitability of CA1 pyramidal neurons by the modulation of voltage-gated ion channels. *Front Cell Neurosci.* 2013;7:91.
- Krzysztoforska K, Mirowska-Guzel D, Widy-Tyszkiewicz E. Pharmacological effects of protocatechuic acid and its therapeutic potential in neurodegenerative diseases: review on the basis of in vitro and in vivo studies in rodents and humans. *Nutr Neurosci.* 2019;22(2):72–82.
- Largo C, Cuevas P, Somjen GG, Martín del Río R, Herreras O. The effect of depressing glial function in rat brain in situ on ion homeostasis, synaptic transmission, and neuron survival. *J Neurosci.* 1996;16(3):1219–1229.
- Lee SH, Dan Y. Neuromodulation of brain states. *Neuron.* 2012;76(1):209–222.
- Lee S, Choi B, Kho A, Jeong J, Hong D, Lee S, Lee M, Lee M, Song H, Choi H, et al. Protective effects of protocatechuic acid on seizure-induced neuronal death. *Int J Mol Sci.* 2018;19(1):187.
- Li X, Li Q, Shi L, Jiao L. Alternating periods of high and low-entropy neural ensemble activity during image processing in the primary visual cortex of rats. *Open Biomed Eng J.* 2016;10(1):51–61.
- Lin CY, Huang CS, Huang CY, Yin MC. Anticoagulatory, antiinflammatory, and antioxidative effects of protocatechuic acid in diabetic mice. *J Agric Food Chem.* 2009;57(15):6661–6667.
- Lipowsky R, Gillissen T, Alzheimer C. Dendritic Na⁺ channels amplify EPSPs in hippocampal CA1 pyramidal cells. *J Neurophysiol.* 1996;76(4):2181–2191.
- López-Aguado L, Ibarz JM, Varona P, Herreras O. Structural inhomogeneities differentially modulate action currents and population spikes initiated in the axon or dendrites. *J Neurophysiol.* 2002;88(5):2809–2820.
- Lörincz ML, Geall F, Bao Y, Crunelli V, Hughes SW. ATP-dependent infra-slow (< 0.1 Hz) oscillations in thalamic networks. *PLoS One.* 2009;4(2):e4447.
- Makarov VA, Makarova J, Herreras O. Disentanglement of local field potential sources by independent component analysis. *J Comput Neurosci.* 2010;29(3):445–457.
- Makarova J, Ibarz JM, Makarov VA, Benito N, Herreras O. Parallel readout of pathway-specific inputs to laminated brain structures. *Front Syst Neurosci.* 2011;5:77.
- Marcaggi P, Mutoh H, Dimitrov D, Beato M, Knöpfel T. Optical measurement of mGluR1 conformational changes reveals fast activation, slow deactivation, and sensitization. *Proc Natl Acad Sci USA.* 2009;106(27):11388–11393.
- Martín-Vázquez G, Benito N, Makarov VA, Herreras O, Makarova J. Diversity of LFPs activated in different target regions by a common CA3 input. *Cereb Cortex.* 2016;26(10):4082–4100.
- Mattison HA, Bagal AA, Mohammadi M, Pulimood NS, Reich CG, Alger BE, Kao JP, Thompson SM. Evidence of calcium-permeable AMPA receptors in dendritic spines of CA1 pyramidal neurons. *J Neurophysiol.* 2014;112(2):263–275.
- Mazzoni A, Whittingstall K, Brunel N, Logothetis NK, Panzeri S. Understanding the relationships between spike rate and delta/gamma frequency bands of LFPs and EEGs using a local cortical network model. *NeuroImage.* 2010;52(3):956–972.
- McGrattan AM, McGuinness B, McKinley MC, Kee F, Passmore P, Woodside JV, McEvoy CT. Diet and inflammation in cognitive ageing and Alzheimer's disease. *Current Nutr Rep.* 2019;8(2):53–65.
- Min S-W, Ryu S-N, Kim D-H. Anti-inflammatory effects of black rice, cyanidin-3-O- β -d-glycoside, and its metabolites, cyanidin and protocatechuic acid. *Int Immunopharmacol.* 2010;10(8):959–966.
- Miyakawa H, Kato H. Active properties of dendritic membrane examined by current source density analysis in hippocampal CA1 pyramidal neurons. *Brain Res.* 1986;399(2):303–309.
- Nadim F, Bucher D. Neuromodulation of neurons and synapses. *Curr Opin Neurobiol.* 2014;29:48–56.
- Nakazono T, Jun H, Blurton-Jones M, Green KN, Igarashi KM. Gamma oscillations in the entorhinal-hippocampal circuit underlying memory and dementia. *Neurosci Res.* 2018;129:40–46.
- Ortuño T, López-Madronea VJ, Makarova J, Tapia-Gonzalez S, Muñoz A, DeFelipe J, Herreras O. Slow-wave activity in the S1HL cortex is contributed by different layer-specific field potential sources during development. *J Neurosci.* 2019;39(45):8900–8915.
- Pazienti A, Galluzzi A, Dasilva M, Sanchez-Vives MV, Mattia M. Slow waves form expanding, memory-rich mesostates steered by local excitability in fading anesthesia. *iScience.* 2022;25(3):103918.
- Picchioni D, Horovitz SG, Fukunaga M, Carr WS, Meltzer JA, Balkin TJ, Duyn JH, Braun AR. Infraslow EEG oscillations organize largescale cortical-subcortical interactions during sleep: a combined EEG/fMRI study. *Brain Res.* 2011;1374:63–72.
- Revueña M, Arteaga O, Montalvo H, Alvarez A, Hilario E, Martínez-Ibargüen A. Antioxidant treatments recover the alteration of auditory-evoked potentials and reduce morphological damage in the inferior colliculus after perinatal asphyxia in rat. *Brain Pathol.* 2016;26(2):186–198.
- Roberts SB, Franceschini MA, Silver RE, Taylor SF, de Sa AB, C6 R, Sonco A, Krauss A, Taetzsch A, Webb P, et al. Effects of food supplementation on cognitive function, cerebral blood flow, and nutritional status in young children at risk of undernutrition: randomized controlled trial. *BMJ.* 2020;370:m2397.
- Román GC, Jackson RE, Gadhia R, Román AN, Reis J. Mediterranean diet: the role of long-chain ω -3 fatty acids in fish; polyphenols in fruits, vegetables, cereals, coffee, tea, cacao and wine; probiotics and vitamins in prevention of stroke, age-related cognitive decline, and Alzheimer disease. *Rev Neurol.* 2019;175(10):724–741.
- Sarkar S. Microglial ion channels: key players in non-cell autonomous neurodegeneration. *Neurobiol Dis.* 2022;174:105861.
- Schmaul S, Hanuscheck N, Bittner S. Astrocytic potassium and calcium channels as integrators of the inflammatory and ischemic CNS microenvironment. *Biol Chem.* 2021;402(12):1519–1530.
- Shimazu R, Anada M, Miyaguchi A, Nomi Y, Matsumoto H. Evaluation of blood-brain barrier permeability of polyphenols, anthocyanins, and their metabolites. *J Agric Food Chem.* 2021;69(39):11676–11686.
- Song J, He Y, Luo C, Feng B, Ran F, Xu H, Ci Z, Xu R, Han L, Zhang D. New progress in the pharmacology of protocatechuic acid: a compound ingested in daily foods and herbs frequently and heavily. *Pharm Res.* 2020;161:105–109.
- Spencer JPE. The impact of flavonoids on memory: physiological and molecular considerations. *Chem Soc Rev.* 2009;38(4):1152–1161.
- Steriade M, Timofeev I, Grenier F. Natural waking and sleep states: a view from inside neocortical neurons. *J Neurophysiol.* 2001;85(5):1969–1985.
- Thakare VN, Dhakane VD, Patel BM. Attenuation of acute restraint stress-induced depressive like behavior and hippocampal alterations with protocatechuic acid treatment in mice. *Metab Brain Dis.* 2017;32(2):401–413.
- Torao-Angosto M, Manasanch A, Mattia M, Sánchez-Vives MV. Up and down states during slow oscillations in slow-wave sleep and different levels of anesthesia. *Front Syst Neurosci.* 2021;15:609645.
- Torres D, Makarova J, Ortuño T, Benito N, Makarov VA, Herreras O. Local and volume-conducted contributions to cortical field potentials. *Cereb Cortex.* 2019;29(12):5234–5254.

- Traub RD, Whittington MA, Jefferys JGR. *Fast oscillations in cortical circuits*. Cambridge: The MIT Press; 1999
- Wang S, Wang B, Shang D, Zhang K, Yan X, Zhang X. Ion channel dysfunction in astrocytes in neurodegenerative diseases. *Front Physiol*. 2022;13:814285.
- Yusufov M, Weyandt LL, Piryatinsky I. Alzheimer's disease and diet: a systematic review. *Int J Neurosci*. 2017;127(2):161–175.
- Zhang YJ, Wu L, Zhang QL, Li J, Yin FX, Yuan Y. Pharmacokinetics of phenolic compounds of Danshen extract in rat blood and brain by microdialysis sampling. *J Ethnopharmacol*. 2011;136(1):129–136.
- Zhang S, Gai Z, Gui T, Chen J, Chen Q, Li Y. Antioxidant effects of protocatechuic acid and protocatechuic aldehyde: old wine in a new bottle. *Evid Based Complement Alternat Med*. 2021;2021:1–19.